CrossMark

RESEARCH PAPER

# Modeling rock specimens through 3D printing: Tentative experiments and prospects

Quan Jiang[1] · Xiating Feng[1] · Lvbo Song[1] · Yahua Gong[1] · Hong Zheng[1] ·
Jie Cui[1]

**Abstract** Current developments in 3D printing (3DP)
technology provide the opportunity to produce rock-like
specimens and geotechnical models through additive man-
ufacturing, that is, from a file viewed with a computer to
a real object. This study investigated the serviceability of
3DP products as substitutes for rock specimens and rock-type
materials in experimental analysis of deformation and failure
in the laboratory. These experiments were performed on two
types of materials as follows: (1) compressive experiments
on printed sand-powder specimens in different shapes and
structures, including intact cylinders, cylinders with small
holes, and cuboids with pre-existing cracks, and (2) com-
pressive and shearing experiments on printed polylactic acid
cylinders and molded shearing blocks. These tentative tests
for 3DP technology have exposed its advantages in produc-
ing complicated specimens with special external forms and
internal structures, the mechanical similarity of its product to
rock-type material in terms of deformation and failure, and
its precision in mapping shapes from the original body to the
trial sample (such as a natural rock joint). These experiments
and analyses also successfully demonstrate the potential and
prospects of 3DP technology to assist in the deformation and
failure analysis of rock-type materials, as well as in the sim-
ulation of similar material modeling experiments.

**Keywords** Rock mechanics · Similar material · 3D
printing · Geotechnical model · Deformation and failure

✉ Quan Jiang
qjiang@whrsm.ac.cn

[1] State Key Laboratory of Geomechanics and Geotechnical
Engineering, Institute of Rock and Soil Mechanics,
Chinese Academy of Sciences, Wuhan 430071, China

## 1 Introduction

Three-dimensional printing (3DP) is also known as addi-
tive manufacturing or additive layer manufacturing. The
3DP facilitates the automated generation of freeform solids
directly from a computer-visional file to a real object [1–3].
Currently, 3DP has been used widely in biological medi-
cine, such as in the building of artificial bone, the migration
of cancer cells, and the construction of engineering tissues
[4–6]; and in subtle electron components, including multi-
functional electronic elements, flipped and embedded chips
[7,8], as well as in lightweight airfoil and satellite parts
[9,10]. Moreover, 3DP has also been utilized in mathematical
visualization, tactile maps, and child education [11–13].

3DP may have wider and explicit application in many dif-
ferent fields. A recent New York Times blog entry referred to
3DP technology as "Industrial Revolution 2.0" [14]. Eisen-
berg compares the invention of 3DP in this century with the
invention of the personal computer in the previous century:
"There are eerie historical echoes here, in the rapid rise of
public interest, between 3D printing in the early 2010's and
home computing in the layer 1970's" [13].

The rapid development of 3DP in terms of manufacturing
and research drives our urgent question: Can 3DP simplify
the experimental study of rock mechanics and rock engineer-
ing? Currently, the laboratory study of rocks, rock mass, and
rock engineering is limited [15–19]. For example, rock sam-
ples obtained from the field are inhomogeneous; thus, making
rock specimens with given artificial cracks or cavities is dif-
ficult, as is producing complicated testing specimens. These
difficulties have hindered the experimental and theoretical
development of rock mechanics. As the traditional study on
geomechanics approaches its limitation, there is a sense of
urgency to find a new pathway to overcome this "bottleneck."

3DP provides us with an alternative because this technology can print specimens with uniform properties and free form. Furthermore, the corresponding computer aided design (CAD) can help produce testing samples with any shape and any flaw.

Therefore, we introduced 3DP into the production of rock specimens and conducted tentative experiments to investigate the serviceability of printed specimens as substitutes for natural rock specimens in experimental deformation and failure studies. These tentative experiments include directly printed specimens with complicated flawed structures and printed molds to indirectly model joined specimens by way of laboratory compressive and shearing tests. The enhanced application prospect of 3DP in the study of rock mechanics and rock engineering is also discussed.

## 2 Material and methods

### 2.1 3DP equipment

Many types of general 3DP equipment and corresponding printing media have been developed based on different formation methods [20]. Among these types of equipment, 3D printers with fused deposition modeling (FDM) and powder-ink binders(PIB) are commonly used.

FDM printers use a print head that acts as an $X - Y - Z$ plotter. During printing, the raw material, which is typically acrylonitrile butadiene styrene (ABS) or biodegradable polylactic acid (PLA), is melted in this print head and deposited layer by layer on the build table to create a 3D object [21–23]. A typical machine and PLA material are shown in Fig. 1. In our experiments, a desktop printer, named Creator, has been applied to the printing PLA model.

PIB printers are based on powder and liquid binders, which are different from the working function of the FDM printers. During each printing cycle, a small thick layer of plaster powder is applied to the model from a supply reservoir. The print head moves across this newly applied layer of powder and spreads the binding agent. The piston in the construction chamber then moves down by the thickness of the layer. The coater applies a new layer of powder, and the process is
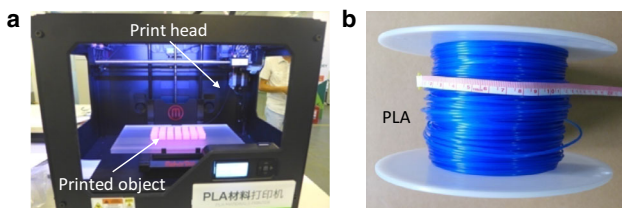


**Fig. 1** General FDM 3D printer and PLA material. **a** FDM printer. **b** PLA material
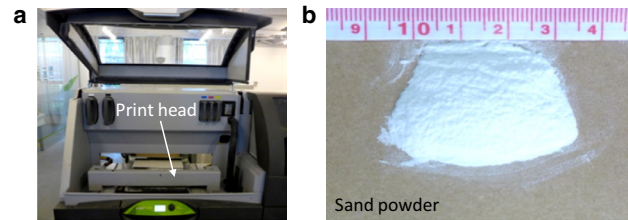


**Fig. 2** General PIB 3D printer and sand-powder material. **a** PIB printer. **b** Sand-powder material

repeated [24, 25]. A representative PIB printer and sand powder material are depicted in Fig. 2. Since the raw material for the PIB printer is the sand powder, its printed products may be more similar intuitively to the rock material. Here, the ProJet X60 printer, a product of the U.S. 3D Systems Corporation, was used for printing the sand-powder specimens in our test.

### 2.2 Printing methodology

Regardless of printer type or material, the general printing process for a model includes the following basic steps:

(1) Model construction. A desired virtual model should first be constructed by a designer using 3D computer-aided software. The CAD model should be identical to the printed model, including its size and shape.
(2) File format conversion. The virtual model file produced based on 3D CAD software must be converted into a format that can be read by the printing software. The standard template library or stereo lithography (STL) format, which describes only the surface geometry of a three-dimensional object without any representation of color, texture or other common CAD model attributes, is the current industry standard for printing models [26, 27]. The STL file represents the model using information about the coordinates and outward surface normal of triangles. At this stage, the technology, which integrates the CAD and computer-aided manufacturing (CAM), has simplified the elaborate process of planning and machine setup.
(3) Model printing. Basic printing parameters, such as filled ratio, printing precision, and layer thickness, should be set after the operating software of the printer has read the virtual model. With sufficient raw printing material, the printing process to directly transform a digital model into a physical object can begin. In our experiment, the filled ratio was set as 100 % for printing the solid model; the printing precision and layer thickness for the FDM printer with PLA material was set as 0.15 and 0.2 mm, respectively; the printing precision and layer thickness

for the PIB printer with sand-powder material was set as 0.1 and 0.2 mm, respectively.

(4) Post-processing. The surface of the printed physical model is not smooth given the precision limitation in 3DP. Thus, the model must often undergo smoothing or strengthening by post-processing. For instance, the final surface of printed cylinder specimens must be rubbed smooth for compressive tests.

## 2.3 Material and specimens for mechanical testing

To test the serviceability of printed specimens as substitutes for natural rock material in the experimental study of geotechnical mechanics and engineering, two types of samples were printed using two materials, respectively; the materials were sand-powder material and PLA material. The specimens constructed with sand powder can be directly used in compressive tests, whereas those generated with the PLA mold can be used as a parent mold for producing physical specimens by filling with other types of similar materials, such as concrete and plaster. Specimens with different flaw structures were also printed to assess their deformational and failure similarities between 3DP material and natural rocks. The sizes of all of the specimens are consistent with the general suggestions of the International Society of Rock Mechanics [28], Fairhurst and Hudson [29]. The virtual 3D models for printing specimens were built by CAD software. The features of the printed specimens are displayed in Fig. 3, and the detailed information of their dimensions is listed in Table 1.
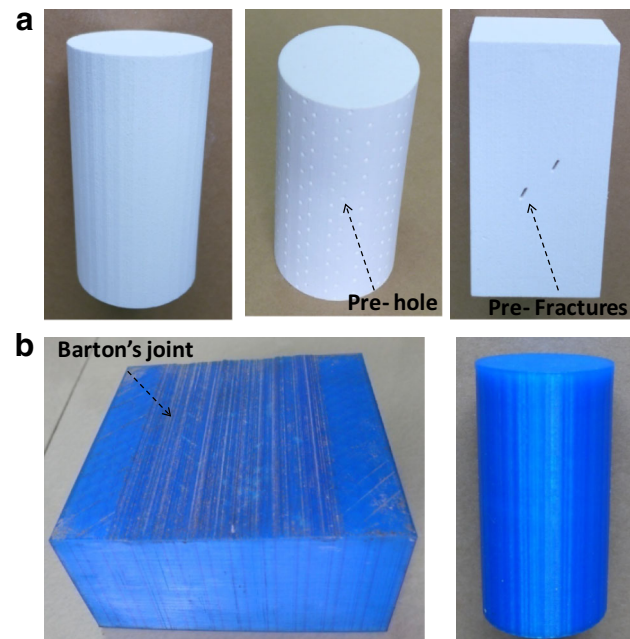


**Fig. 3** 3DP specimens for experiment. **a** Sample produced by sand-powder material. **b** Sample produced by PLA material

## 3 Mechanical compression test on sand-powder specimens

The geotechnical mechanics-based approach to solving problems with rock mechanics requires prior knowledge of rock stress–strain behavior. Important aspects of this behavior generally include the constants related to stresses and strains in the elastic range; the stress levels at which yield, fracturing, or slip occurs within the rock; and the post-peak stress–strain behavior of fractured or failed rocks [29]. Thus, mechanical compression tests for the 3DP specimens are necessary for the purpose of applying the 3DP technology in the further study of geotechnical mechanics and engineering.

To investigate the identical and dissimilar traits between the sand-powder 3DP model and natural rock in deformation and failure mode, basic compressive tests were conducted on 3DP specimens in several shapes. These experiments included the uniaxial and triaxial compression for the intact 3DP cylinder specimens; the uniaxial compressions for the 3DP cylinder specimens with small holes, and the cuboid specimens with single or double cracks.

### 3.1 Compressive test of the intact cylinder 3DP specimen

These trial works were performed with the electro-hydraulic servo-controlled rock mechanics testing system (MTS-815). During testing, the loading mode was initiated through displacement control with a ratio of 0.002 mm/s, and the axial strain was measured using a linear variable differential transformer (LVDT). During the stable uniaxial loading process, the axial stress of the sand-powder specimens first increased approximately linearly with the axial strain before peaking (Fig. 4). The axial stress subsequently decreased after peaking, although the axial strain continued to increase and exhibit strain-softening behavior. Finally, the axial stress reached a low and stable stress level under continued load from MTS. In sum, the integrated axial strain–stress curve of the 3DP specimen included the elastic, strain-softening, and residual parts that displayed characteristic peaks and residual stresses. The axial strain–stress characteristics of the sand-powder 3DP model under uniaxial compression was similar to those of generic rock material [30–32].

In addition, the lateral strain and volumetric strain curves of the printed sand-powder specimen in Fig. 4 are also similar to the compressive deformation properties of natural rock. In particular, the lateral strain of the 3DP specimen increased linearly with axial loading stress before the stress peaked. However, this strain then increased rapidly and nonlinearly (i.e., dilatation) when the loading stress was near and exceeded peak strength. Moreover, the volumetric strain displayed as bulk shrinkage before the stress peak and rapid bulk expansion after stress peak. This dilatation effect exerted by

**Table 1** Basic characteristics of simulated rock specimens manufactured by 3D printer

| Raw material | Specimen type | Dimension parameters | Printing resolution (mm) | Density (Kg/m$^3$) |
|---|---|---|---|---|
| Sand powder | Cylinder | 50 mm in diameter and 100 mm in height | 0.1 | $1.26 \times 10^3$ |
| | Cylinder with holes | Cylinder with 50 mm in diameter and 100 mm in height; holes with 2 mm in diameter and 5 mm in space | | |
| | Cuboid with cracks | Cuboid with edges in 50, 50, 100 mm; Crack with 5 mm in length and 10 mm in space | | |
| PLA | Cylinder | 35 mm in diameter and 70 mm in height | 0.15 | $0.758 \times 10^3$ |
| | Joint mould | Edges in 10 cm, contain Barton's standard joint, JRC = 6–8 [43] | | |
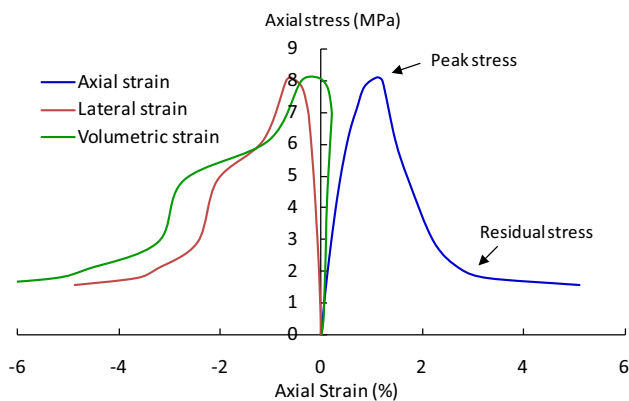


**Fig. 4** Typical full stress–strain curves of the 3DP sand-powder specimen under uniaxial compression

the printed sand-powder specimen also mimicked the lateral and volumetric deformation features of rocks.

Further investigation into the failure plane of the failed 3DP specimens indicated the presence of several vertical tensile cracks on the cylinder under uniaxial compression (Fig. 5a), but only one main shearing plane under relative high confining stress (1.0 MPa). The break features of printed specimens were also similar to the failure behavior of generic rocks, such as the tensile splitting breakage of marble under uniaxial compression and shearing breakage under triaxial compression with high confining stress (Fig. 5b).

### 3.2 Uniaxial compression of the printed specimen with holes

Although defects within the rock, including pores, flaws, and cracks, considerably affect its macro mechanical properties, rock specimens with given holes or flaws, such as amygdaloidal basalt, remain difficult to obtain in laboratory tests.
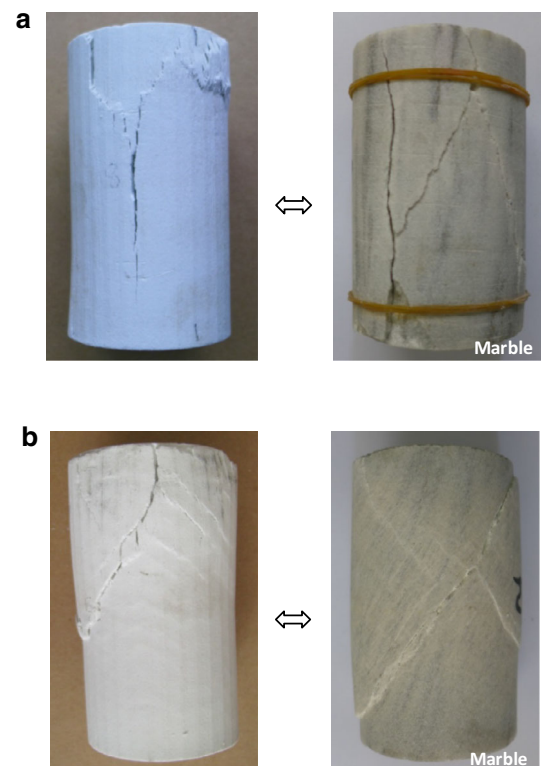


**Fig. 5** Comparison of the break planes of the failed 3DP specimens and of actual rock samples. **a** Tensile break under uniaxial compression. **b** Shearing break under confining stress

The new 3DP technology can easily overcome this challenge by printing virtual CAD models as realistic specimens. In this study, we manufactured a 3DP cylinder sample with regular holes that were 2 mm in diameter and positioned 5 mm apart (see Fig. 3) to illustrate the advantages of this technology. The stress–strain curves of this type of printed specimens, which were also under uniaxial compression, were presented
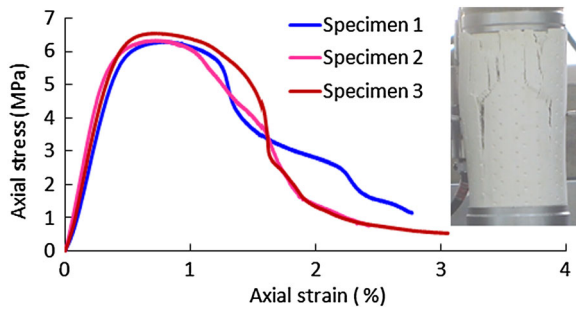
**Fig. 6** Stress–strain curves of printed specimens with holes



**Fig. 7** Fracture extension in the 3DP specimen with pre-existed cracks under uniaxial compression

as linear elastic deformations before yield and displayed a clear peak strength phase and strain-softening behavior after peak stress (Fig. 6). Moreover, the compressive stress–strain curves of the three specimens were similar to one another before the peak stress. These findings showed that the specimens produced by the 3D printer were uniform in terms of deformation properties. The deviation of specimens' axial stress, strain curves after peak stress, also indicated that the small holes inside the specimens might have had an effect on the uncertainty of the crack extensions.

The uniaxial compressive strength of specimens with holes was lower than that of intact specimens, i.e., lower than approximately 23.6% of the intact specimens. This fact also confirmed the general knowledge that the defects in rock-type material would decrease its loading capability. Furthermore, this simple experiment on the printed sample with holes and its typical results demonstrated the ease of constructing defected samples using CAD and 3DP technologies.

### 3.3 Observation of fractures in printed cuboid specimens with pre-existing cracks

Joints and micro fractures are commonly found in natural rocks, and their failure mechanism depends strongly on the pattern of extension and coalescence in cracks between pre-existing flaws and the rock-bridge area. Numerous studies have examined physical model blocks through artificially pre-existing fractures [33–36]. During their work, there was still difficulty in creating one or several pre-existing cracks before experimental study. Yet, this generation process can be simplified by conceptualizing a virtual specimen with special cracks on a computer using the CAD method. The 3D printer can then easily manufacture a given sample with 2D or 3D cracks, which can differ in terms of individual shape and combinational relationship. To test the efficiency and effectiveness of the 3DP method in modeling rock specimens with pre-existing cracks, several cuboid specimens containing one or two 2D through-going cracks were first built, and the cor-
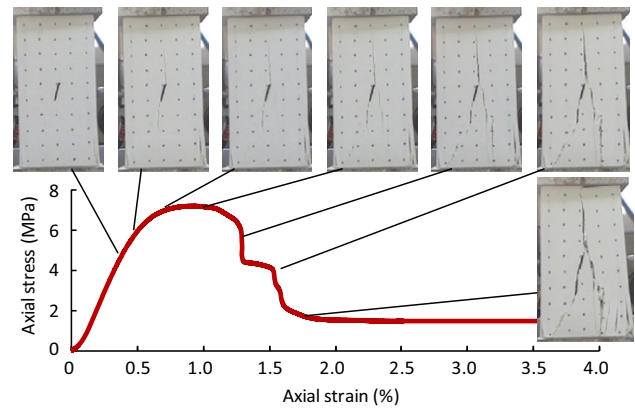
responding compressive tests whose loading condition is the same with the cylinder specimens were conducted.

During the uniaxial compression experiment, new cracks first appeared at the tip of the existing cracks and subsequently extended gradually when the loading stress approached the specimen's peak strength (Fig. 7). The subsequent load on the specimen drove the continued extension of current cracks in a wing-like manner and initiated new cracks. This time-dependent cracking process of this specimen also can be drawn according to the axial loading ratio and the axial strain in Fig. 7. This phenomenon embodied the macro strain-softening behavior and eventual structural disintegration of the specimen. The crack extension corresponded with the experimental findings of Wong [37] and Zhang [38] regarding the fracturing behaviors of real rocks with pre-existing cracks.

Furthermore, the final failure form of the 3DP cuboid specimens containing one or two pre-existing cracks were similar to that of the rock material in the failure model, especially with respect to the fracture extension at pre-existing crack tips and the coalescence among cracks. A parallel comparison of the fracturing phenomena in printed sand-powder specimens and in real rock-type samples is displayed as in Fig. 8 by referencing experimental results [19,34]. For example, both the extending direction of the wing crack at the tip of the pre-existing crack and the shearing failure of the "rock bridge" between two pre-existing cracks were similar to each other between the printed sand-powder specimens and real rock samples.

The compressive tests on the intact and defective samples displayed mechanical performance that was similar to the general behavior of rock-type materials. The results from these tentative experiments also suggest that 3DP technology can manufacture experimental samples with various structures and shapes. That means this technology can provide many opportunities for applying it in geotechnical study on mechanical mechanisms and actual engineering.
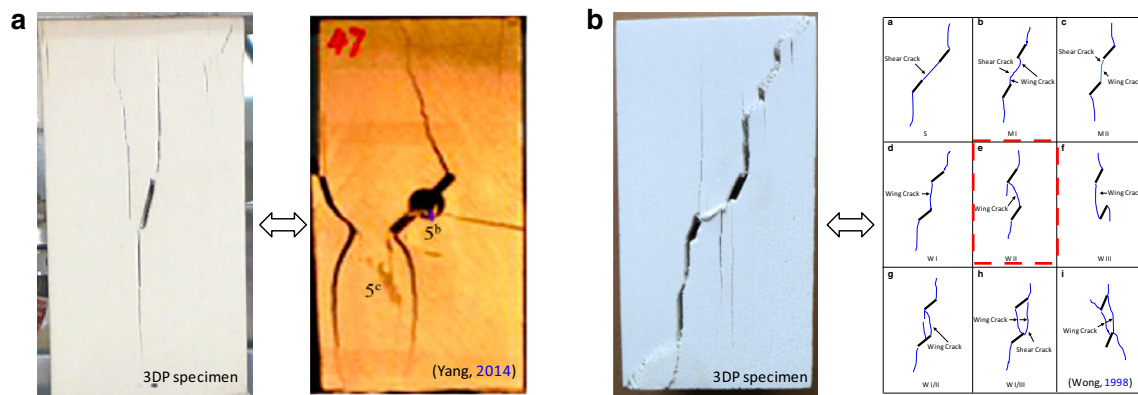
**Fig. 8** Comparison of fracturing phenomena in 3DP sand-powder specimens and in actual rock-type samples. **a** Fractured sandstone specimen with a single pre-existed crack. **b** Fractured specimen with double pre-existed cracks

## 4 Mechanical test on the PLA material

A number of PLA cylinders were also tested through uniaxial compression to investigate their basic compressive property. The working parameters of the MTS-815 testing system were set as the same as that for the sand-powder specimens. For checking the usefulness of the printed PLA mold in producing a joint sample with the same joint surface, direct shearing tests were conducted, which were performed by injecting a similar concrete on the PLA mold.

### 4.1 Uniaxial compression for the PLA cylinder

During the uniaxial compressive test on the PLA specimens, the axial stress increased with the axial strain linearly before the loading stress was lower than its yield strength. However, when the successive loading stress reached yield stress, the axial stress of the compressed PLA specimen reached a stable level. This behavior indicated that the PLA approximated an elasto-plastic material (Fig. 9). The compressive test results also implied that the yield PLA specimen did not display a local shearing band, but exhibited plastic drum expansion. The mechanical performance of the PLA differed signifi-
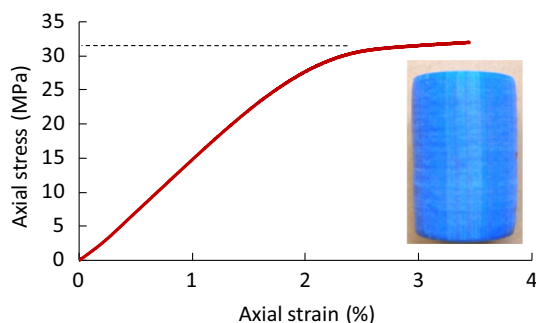
cantly from that of the rock material, but it was similar to that of metal material. Therefore, we can use the PLA mold manufactured by the 3D printer to model either the rock bolt or the supporting shell for tunneling experiments conducted with physical modeling in the laboratory.

### 4.2 Direct shearing test on the modeling joint

Obtaining a sufficient number of joint specimens with identical joint shapes is a traditional challenge in shearing and compressive experiments [39–42]. However, 3DP technology can be used to conveniently generate a visual 3DP joint mold through CAD, based on the obtained joint data. This visual mold can then be printed into an actual PLA mold with the desired joint shape. Finally, physical joint specimens can be generated by injecting special concrete or other similar material into this PLA mold. Given that these physical specimens are produced using the same PLA mold, their joint shape must be highly similar.

To demonstrate the practicality of the aforementioned method, a PLA mold that contains a standard Barton's joint [43] was first printed. The JRC value of this joint was approximately 6–8. Some specimens can then be molded based on the PLA body by pouring matched concrete with the 10.7GPa mold onto the joint surface of the PLA mold, as shown in Fig. 10a. By way of 3D scanning for the physical concrete model and corresponding interpolation deal for the gained digital surface data, the 2D profile lines at given positions can be obtained. Analysis of the 2D profile lines of the physical model indicated that its joint roughness coincided significantly with the original Barton's joint (Fig. 10b). These concrete specimens had been sheared under the special experiment machine for testing their shearing performance. The results of an additional direct shearing test on these specimens suggest that their shearing stress-displacement curves fit one another perfectly under uniform experimental conditions (Fig. 11). Therefore, shape analysis and mechanical



**Fig. 9** Stress–strain curve of the PLA specimen under uniaxial compression test and its failed form
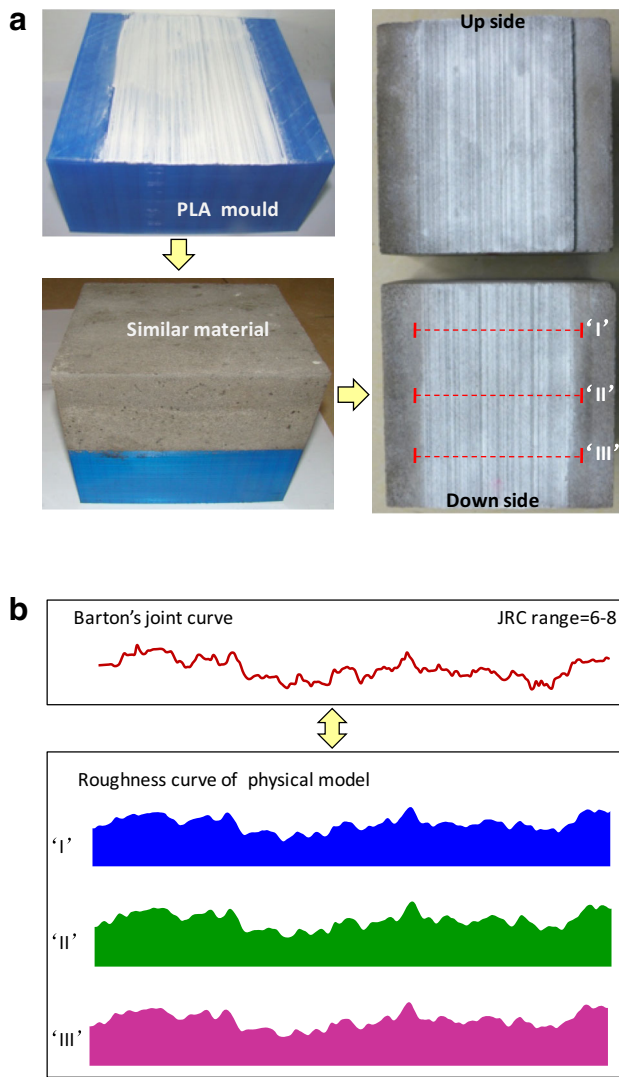
Fig. 10 Modeling a physical specimen with Barton's joint surface using a PLA mold. **a** Modeling process starting from the PLA mold to the generation of a concrete specimen. **b** Comparison of the original Barton's joint curve and the actual joint shape on the concrete specimen
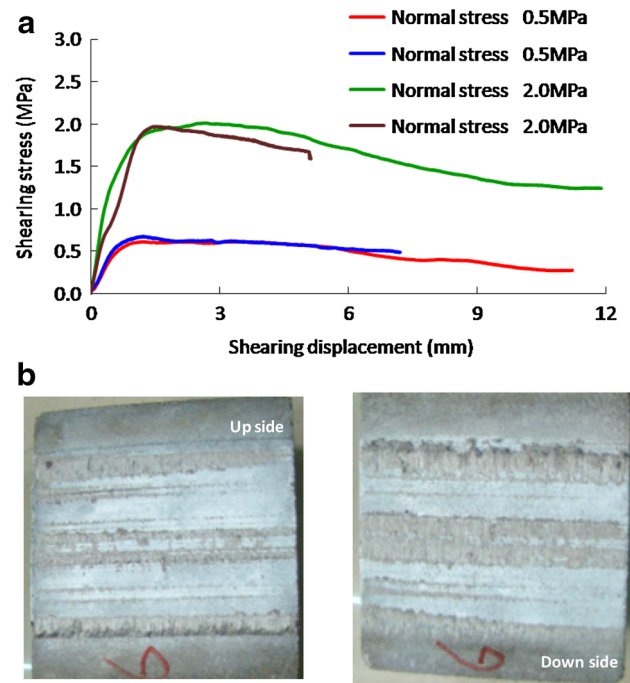


Fig. 11 Shearing test for the concrete specimen containing Barton's joint. **a** Shearing stress-displacement curves under different normal stress. **b** Sheared surfaces of the specimen

shearing tests on the generated specimens indicated that the printed PLA mold can copy the joint shape with high accuracy.

Furthermore, the shearing specimens containing a natural rock joint can also be constructed by integrating the 3D scanning technology with the 3DP technology (Fig. 12). First, we obtained the point cloud data of a natural joint surface using a 3D scanning machine. We then constructed a virtual joint model based on the scanning data and printed a real PLA model that included precisely shaped natural joints. Before printing, the virtual joint model constructed using computer aided design needs to be converted to a standard STL format, which is readable by the 3D printing software. Basic printing parameters, such as the filled ratio, printing precision,

layer thickness, etc., should be set before the printer's operating software reads the virtual model. Thus, some artificial physical models for experiments can be built with this PLA mold according to the aforementioned method. Typically, experimental curves between the shearing force and shearing displacement had been gained also based on the shear test for these specimens containing natural rock joints (Fig. 13).

## 5 Prospective discussion of 3DP in geotechnical mechanics and engineering

The results of the experiments above had shown that the strain–stress behavior of the printed sand-powder specimens was similar to the common behavior of natural rock under compressive testing. Its cracking propagation was also similar to that of rock-type materials. The findings of shearing tests on concrete joint specimens constructed using the printed PLA mold also indicated that the roughness of these specimens was highly similar. Corresponding experimental data suggested that the joint specimens modeled with the printed PLA mold were completely identical to one another. Moreover, the results of the uniaxial compressive test for the PLA cylinder implied that its elasto-plastic mechanical property resembled that of metal. Further development of 3DP technology will certainly provide increased opportunity for us to extend its application in rock mechanics and
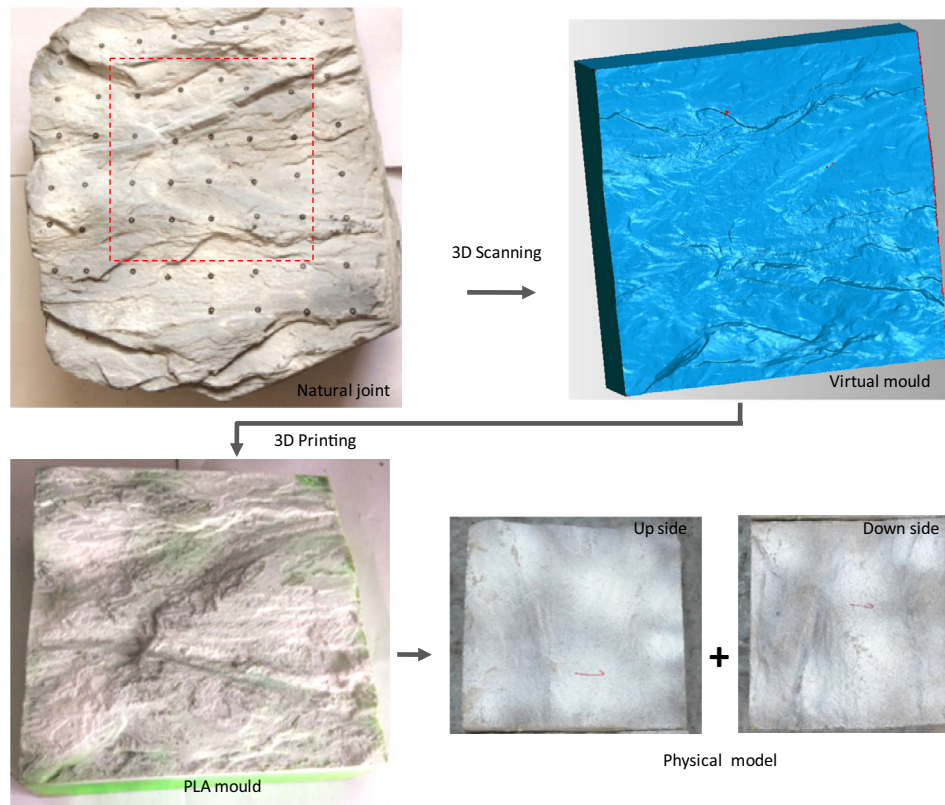
**Fig. 12** Technical process of the generation of an artificial specimen with natural joints based on the 3D scanning and 3DP
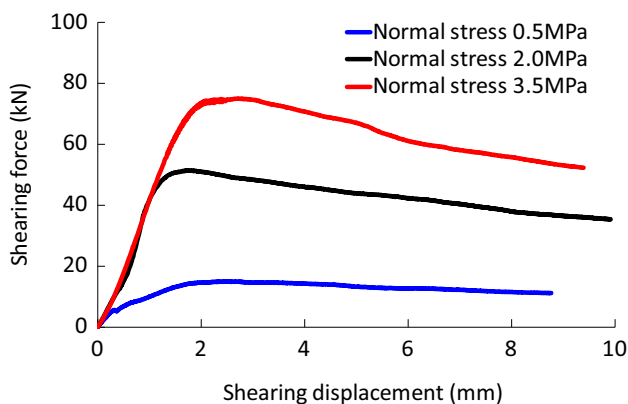


**Fig. 13** Typical experimental curves of the specimens containing a natural rock joint based on the shear test

engineering with the aid of an affinity theory for model testing, although its application in geotechnical mechanics and engineering is only in tentative ways.

## 5.1 Potential application of 3DP

The 3DP can directly and simply convert conceptualized models into physical models. Thus, we can produce rock-like specimens in given shapes and strengths for special experimental study purposes regardless of the difficulty of processing testing samples. The foreseeable applications and effects of 3DP may include the following (Fig. 14).

(1) Printing rock-like specimens. Rock-like specimens can be printed in different shapes, such as cylinders, cuboids, and hollow cylinders. They can also be printed with special local structures, such as holes, cracks, interlayers, and seepage piping. The printed specimens can be used in different experimental tests, such as compressive testing, tensile testing, and three-point bending. Moreover, these specimens can be generated with set values for elasticity modulus, Poisson ratio, cohesion strength, and fractional angle by adjusting the mixed ingredients with the development of printing material and 3DP technology progress.

(2) Printing models with similar materials. 3DP can be used to overcome the difficulty of generating complicated physical models by direct manufacturing during analog simulation experiments. Such models include analog physical models with tunnels or crossed caverns [44,45], slopes or landslides with natural surfaces [46,47], and foundation trench models with support structures, etc.

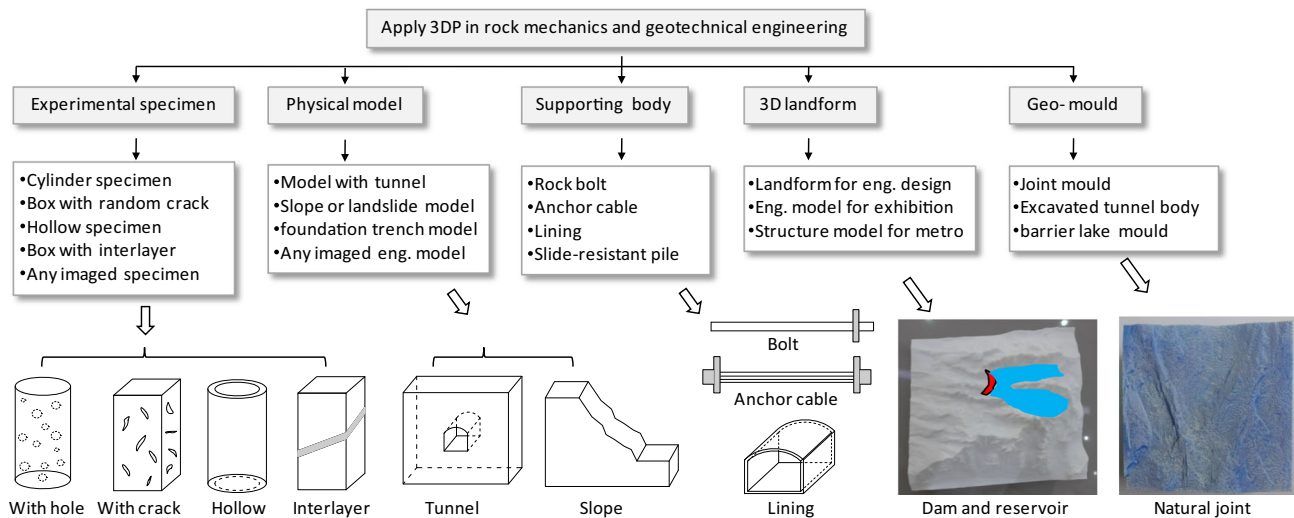(3) Printing support units. Actual supporting tools for geotechnical engineering, such as rock bolts, anchor

**Fig. 14** 3DP application in rock mechanics and geotechnical engineering

cables, linings, and piles, can be printed directly in any given size and shape without material waste or re-treatment. Moreover, small supporting elements can also be produced using a 3DP machine for similar physical tests.

(4) Printing 3D land forms for pre-engineering designs. Printed 3D landforms can be used to optimize the analysis of overall arrangement designs prior to construction, to realize engineering designs, or to manage geo-disaster relief efforts.

(5) Printing geo-molds. Certain geo-modules, such as natural rock joints, can be printed according to captured digital models. Geo-bodies, such as barrier lakes, can also be printed to simulate flood discharge risk.

## 5.2 Current limitations of the 3DP technique

Current 3DP techniques remain limited in terms of experimental rock mechanics despite their clear advantages. Thus, they should be improved and developed further in the following ways to enhance their role in geotechnical and mechanical engineering:

(1) The printing material must be improved to resemble natural rock. Current printing materials, such as sand powder, PLA, ABS, silicon rubber, glass-filled nylon, and metal powder, limit the capability of 3DP technology to simulate rock-like materials with uniform strength. For example, current rock-like specimens printed from sand-powder material only have a compressive strength of less than 10 MPa. That of the elastic modules is approximately 2 GPa, although some ceramic samples are strong and display large module values. However, most rocks have a compressive strength of more than 30 MPa, and even more than 100 MPa. Thus, a new rock-like material with high compressive strength, low tensile strength, brittle failure property and frictional function must be explored for the printing of artificial rock-like specimens.

(2) The function of 3D printers must be developed further. The current product by 3DP is generally less than 1 m in size. This size cannot satisfy the need to produce intact physical models that are often tens of meters in size for rock engineering, although it can provide general specimens for laboratory experiments. Moreover, most existing printers have only one or two printing nozzles; thus they can print only one or two materials. However, actual rock masses are heterogeneous in terms of mechanical properties. Therefore, a printer that produces several materials must be developed so that specimens can be printed with the expected strength, module, and Poisson ratio.

Nonetheless, these temporary shortcomings do not nullify the application potential of 3DP in the geotechnical field. Thus, we remain confident in its capability. At present, the theory of similar simulation can help partially address the limitations of printed samples in terms of mechanical strength and shape size [48–50]. Furthermore, we also believe that the advancement of 3DP technology can overcome its shortcomings to promote the study of rock mechanics and engineering in the coming years.

## 6 Conclusions

The development and popularization of 3DP technology have provided the opportunities for us to apply it in geotech-

nical mechanics and engineering. This study successfully demonstrated the potential of 3DP technology to assist in the deformation and failure analysis of rock-type materials and in the simulation of similar material modeling experiments.

The tentative printing tests with the sand-powder material verified that 3DP technology can produce specimens with any external shape and pre-existing defect. The results of subsequent mechanical experiments of these specimens indicated that not only were their compressive stress–strain curves similar to those of generic rock, but that their fracture characteristics and crack extensions were also similar to the failure of rock-type materials. Moreover, the direct shearing test on the concrete joint constructed with a printed PLA mold confirmed the advantages of 3DP technology in producing experimental specimens with natural and artificial joints.

The 3DP offers an unconventional method for producing patterns of experimental specimens and similar material models. Furthermore, the results of the tentative experiments of the 3DP samples demonstrated that this new technology can be applied to study the mechanical mechanisms of rock-type materials. We optimistically believe that the development of 3DP technology will extend its function in geotechnical mechanics and engineering, including producing experimental specimens, printing geotechnical engineering, manufacturing supporting units, and exhibiting landform and engineering layout models. The extension of the 3DP method would promote the development of geomechanics and may initiate a new branch in traditional rock mechanics.

# References

1. Charles, H.: Apparatus for production of three-dimensional objects by stereolithography. U.S. Patent 4,575,330 (1986)
2. Sachs, E.M., Haggerty, J.H., Cima, M.J., et al.: Three-dimensional printing techniques, US Patent 5,204,055. (1989)
3. Wohlers, T., Gornet, T.: History of additive manufacturing. Online Supplement to wohlers report 2011. http://www.wohlersassociates.com/history2011, Accessed 22.3.2012. (2012)
4. Yoo, S.S.: 3D On-Demand Bioprinting for the Creation of Engineered Tissues. In: Ringeisen, B.R., et al. (eds.) Cell and Organ Printing, pp. 3–17. Springer Science Business Media B.V, New York (2010)
5. Bose, S., Vahabzadeh, S., Bandyopadhyay, A.: Bone tissue engineering using 3D printing. Mater. Today **16**, 496–504 (2013)
6. Huang, T.Q., Qu, X., Liu, J., et al.: 3D printing of biomimetic microstructures for cancer cell migration. Biomed. Microdevices **16**, 127–132 (2014)
7. Espalin, D., Muse, D.W., MacDonald, E., et al.: 3D Printing multifunctionality: structures with electronics. Int. J. Adv. Manuf. Technol. **72**, 963–978 (2014)
8. Hoerber, J., Glasschroeder, J., Pfeffer, M., et al.: Approaches for additive manufacturing of 3D electronic applications. Procedia CIRP **17**, 806–811 (2014)
9. Lyke, J.C.: Plug-and-play satellites. IEEE Spectr. **49**, 36–42 (2012)
10. Moon, S.K., Tan, Y.E., Hwang, J., et al.: Application of 3D printing technology for designing light-weight unmanned aerial vehicle wing structures. Int. J. Precis. Eng. Man. Gr. Technol. **1**, 223–228 (2014)
11. Henry, S.: 3D Printing for mathematical visualisation. In: Michael, K., Ravi, V. (eds.) Mathematical Entertainments, pp. 56–62. University of California, Berkeley (2012)
12. Schwarzbach, F., Sarjakoski, T., Oksanen, J., et al.: Physical 3D models from LIDAR data as tactile maps for visually impaired persons. In: Buchroithner, M. (ed.) True-3D in Cartography: Auto Stereoscopic and Solid Visualisation of Geodata, Lecture Notes in Geoinformation and Cartography. Springer, Berlin (2012)
13. Eisenberg, M.: 3D printing for children: What to build next? Int. J. Child Comput. Interact. **1**, 7–13 (2013)
14. Bilton, N.: The 3-D Printing Free-for-All. (2011)
15. Priest, S.D., Brown, E.T.: Probabilistic stability analysis of variable rock slopes. Trans. Inst. Min. Metall. A. **92**, 1–12 (1983)
16. Hoek, E.: Reliability of Hoek-Brown estimates of rock mass properties and their impact on design. Int. J. Rock Mech. Min. Sci. **35**, 63–68 (1998)
17. Cai, M.: Rock Mass Characterization and rock property variability considerations for tunnel and cavern design. Rock Mech. Rock Eng. **44**, 379–399 (2011)
18. Manouchehrian, A., Marji, M.F.: Numerical analysis of confinement effect on crack propagation mechanism from a flaw in a pre-cracked rock under compression. Acta Mech. Sin. **30**, 547–558 (2014)
19. Yang, S.Q., Jing, H.W., Xu, T.: Mechanical behavior and failure analysis of brittle sandstone specimens containing combined flaws under uniaxial compression. J. Cent. South Univ. **21**, 2059–2073 (2014)
20. Niewiadomski, R., Anderson, D.: 3-D manufacturing: The beginning of common creativity revolution. In: Lee, N. (ed.) Digital Da Vinci. Springer Science Business Media, New York (2014)
21. McMains, S.: Layered manufacturing technologies. Commun. ACM **48**, 50–55 (2005)
22. Herrmann, K.H., Gartner, C., Gullmar, D., et al.: 3D printing of MRI compatible components: Why every MRI research group should have a low-budget 3D printer. Med. Eng. Phys. **36**, 1373–1380 (2014)
23. Bell, C.: The possibility maintaining and troubleshooting your 3D printer. Technology in action, Friends of Apress (2014)
24. Jee, H.J., Sachs, E.: A visual simulation technique for 3D printing. Adv. Eng. Softw. **31**, 97–106 (2000)
25. Junk, S., Samann-Sun, J., Niederhofer, M.: Application of 3D printing for the rapid tooling of thermoforming moulds. In: Lin, L. (ed.), Proceedings of the 36th International MATADOR Conference, SrichandHinduja, pp, 369–372 (2010)
26. Serrat, J., Lumbreras, F., Lopez, A.M.: Cost estimation of custom hoses from STL files and CAD drawings. Comput. Ind. **64**, 299–309 (2013)
27. Wikipedia: STL (file format). http://en.wikipedia.org/wiki/STL_(file_format)#cite_ref-1. Accessed 22.3.2012 (2015)
28. ISRM.: Suggested methods for determining the uniaxial compressive strength and deformability of rock materials. Int. J. Rock Mech. Min. Sci. Geomech. Abs. **16**, 135–140 (1979)
29. Fairhurst, C.E., Hudson, J.A.: Draft ISRM suggested method for the complete stress-strain curve for intact rock in uniaxial compression. Int. J. Rock. Mech. Min. Sci. **36**, 279–289 (1999)
30. Brady, B.H.G., Brown, E.T.: Rock Mechanics for Underground Mining, 3rd edn. Springer Science Inc., Boston (2004)

31. Cai, M.: Practical estimates of tensile strength and Hoek-Brown strength parameter mi of brittle Rocks. Rock Mech. Rock Eng. **43**, 167–184 (2010)

32. Jiang, Q., Feng, X.T., Hatzor, Y.H., et al.: Mechanical anisotropy of columnar jointed basalts: An example from the Baihetan hydropower station. China. Eng. Geol. **175**, 35–45 (2014)

33. Bobet, A., Einstein, H.H.: Fracture coalescence in rock-type materials under uniaxial and biaxial compression. Int. J. Rock. Mech. Min. Sci. **35**, 863–888 (1998)

34. Wong, R.H.C., Chau, K.T.: Crack coalescence in a rock-like material containing two cracks. Int. J. Rock Mech. Min. Sci. **35**, 147–164 (1998)

35. Zhang, Z.H., Sun, F.: The three-dimension model for the rock-breaking mechanism of disc cutter and analysis of rock-breaking forces. Acta Mech. Sin. **28**, 675–682 (2012)

36. Wasantha, P.L.P., Ranjith, P.G., Xu, T., et al.: A new parameter to describe the persistency of non-persistent joints. Eng. Geol. **181**, 71–77 (2014)

37. Wong, R.H.C., Chau, K.T., Tang, C.A.: Analysis of crack coalescence in rock-like materials containing three flaws—part I: experimental approach. Int. J. Rock. Mech. Min. Sci. **38**, 909–924 (2001)

38. Zhang, X.P., Wong, L.N.Y., Wang, S.J.: Effects of the ratio of flaw size to specimen size on cracking behavior. B. Eng. Geol. Environ. **74**, 181–193 (2015)

39. Haberfield, C.M., Seidel, J.P.: Some recent advances in the modelling of soft rock joints in direct shear. Geotech. Geol. Eng. **17**, 177–195 (1999)

40. Ghazvinian, A.H., Taghichian, A., Hashemi, M., et al.: The Shear behavior of bedding planes of weakness between two different rock types with high strength difference. Rock Mech. Rock Eng. **43**, 69–87 (2010)

41. Usefzadeh, A., Yousefzadeh, H., Hossein, S.R.: Empirical and mathematical formulation of the shear behavior of rock joints. Eng. Geol. **164**, 243–252 (2013)

42. Yang, S.Q., Huang, Y.H.: Particle flow study on strength and meso-mechanism of Brazilian splitting test for jointed rock mass. Acta Mech. Sin. **30**, 547–558 (2014)

43. Barton, N., Choubey, V.: The shear strength of rock joints in theory and practice. Rock Mech. **10**, 1–54 (1997)

44. Sterpi, D., Cividini, A.: A Physical and numerical investigation on the stability of shallow tunnels in strain softening media. Rock Mech. Rock Eng. **37**, 277–298 (2004)

45. Li, Y.J., Zhang, D.L., Fang, Q., et al.: A physical and numerical investigation of the failure mechanism of weak rocks surrounding tunnels. Comput. Geotech. **61**, 292–307 (2014)

46. Xu, X.N., Chen, Y.L., Li, S.W.: Study of shock landslide-Type geomechanical model test for consequent rock slope. In: Margottini, C. (ed.) Landslide Science and Practice, pp. 11–16. Springer, Berlin (2014)

47. Chen, G.Q., Huang, R.Q., Xu, Q., et al.: Progressive modelling of the gravity-induced landslide using the local dynamic strength reduction method. J. Mt. Sci. **10**, 532–540 (2013)

48. Fumagalli, E.: Statically and Geomechanical Models. (Translated by P.N. Jang)., China Water Resources and Electric Power Press, Beijing (1979)

49. Meguid, M.A., Saada, O., Nunes, M.A., et al.: Physical modeling of tunnels in soft ground: a review. Tunn. Under Sp. Tech. **23**, 185–198 (2008)

50. Chen, G.Q., Li, T.B., Zhang, G.F., et al.: Temperature effect of rock burst for hard rock in deep-buried tunnel. Nat. Hazards **72**, 915–926 (2014)